Substrate diffusion and oxidation in GMC oxidoreductases: An experimental and computational study on fungal aryl-alcohol oxidase

Aitor Hernández-Ortega, Kenneth Borrelli, Patricia Ferreira, Milagros Medina, Angel T. Martinez, Victor Guallar

Biochemical Journal Immediate Publication. Published on 04 Mar 2011 as manuscript BJ20102090

Substrate diffusion and oxidation in GMC oxidoreductases: An experimental and computational study on fungal aryl-alcohol oxidase

Aitor HERNÁNDEZ-ORTEGA*[1], Kenneth BORRELLI†[1], Patricia FERREIRA‡, Milagros MEDINA‡, Angel T. MARTÍNEZ*[2] and Victor GUALLAR†[2]

*Centro de Investigaciones Biológicas, Consejo Superior de Investigaciones Científicas (CSIC), Ramiro de Maeztu 9, E-28040 Madrid, Spain, †Catalan Institution for Research and Advanced Studies, Barcelona Supercomputing Center, Edificio Nexus II, E-08028 Barcelona, Spain ‡Department of Biochemistry and Molecular and Cellular Biology and Institute of Biocomputation and Physics of Complex Systems, University of Zaragoza, E-50009 Zaragoza, Spain

Short title: Substrate diffusion and oxidation in AAO

Aryl-alcohol oxidase (AAO) provides H_2O_2 in fungal degradation of lignin, a process of high biotechnological interest. Its crystal structure does not show an open access to the active site, where different aromatic alcohols are oxidized. We studied substrate diffusion and oxidation in AAO, compared with the structurally-related choline oxidase (CHO). Cavity finder and ligand diffusion simulations indicate the substrate entrance channel, requiring side-chain displacements and involving a stacking interaction with Tyr^{92}. Mixed quantum mechanics/molecular mechanics (QM/MM) studies combined with site-directed mutagenesis showed two active-site catalytic histidines, whose substitution strongly decreased both catalytic and (transient-state) reduction constants for *p*-anisyl alcohol in the H502A (over 1800-fold) and H546A (over 35-fold) variants. Combination of QM/MM energy profiles, protonation predictors, molecular dynamics, mutagenesis, and pH profiles give a robust answer about the nature of the catalytic base. The histidine in front of the FAD ring, AAO His^{502} (and CHO His^{466}), acts as a base. For the two substrates assayed, it was shown that proton transfer preceded hydride transfer, although both processes are highly coupled. No stable intermediate was observed in the energy profiles, in contrast with that observed for CHO. QM/MM, together with solvent KIE results, suggest a non-synchronous concerted mechanism for alcohol oxidation by AAO.

Key words: aryl-alcohol oxidase (AAO), catalytic base, GMC oxidoreductases, molecular docking, quantum mechanics/molecular mechanics (QM/MM), reaction mechanisms

INTRODUCTION

Aryl-alcohol oxidase (AAO; EC 1.1.3.7) catalyzes the oxidation of aromatic, and some aliphatic polyunsaturated, alcohols with the concomitant production of H_2O_2 [1] involved in lignin biodegradation in a reaction catalyzed by high redox-potential peroxidases [2]. Lignin removal is a key step for carbon recycling in land ecosystems, and a key issue for the industrial use of plant biomass in lignocellulose biorefineries, where biotechnology will contribute to the sustainable production of biofuels, chemicals and other products [3]. The AAO overall reaction involves a polyunsaturated alcohol, with a primary hydroxyl at the α-carbon, and O_2 in presence of a FAD enzyme cofactor:

[1] A.H.-O. and K.B. contributed equally to this work.

[2] To whom correspondence should be addressed (Victor Guallar, Tel 34 934137727, Fax 34 934137721, E-mail: victor.guallar@bsc.es; and Angel T. Martínez, Tel 34 918373112, Fax 34 915360432; E-mail atmartinez@cib.csic.es).

Abbreviations used: AAO, aryl-alcohol oxidase; CHO, choline oxidase; DFT, density functional theory; GMC, glucose-methanol-choline oxidases; KIE, kinetic isotope effect; MD, molecular dynamics; MM, molecular mechanics; QM, quantum mechanics.

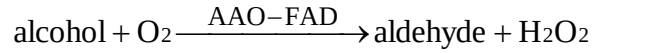

After gene cloning [4] homology modelling of AAO revealed common features with members of the GMC (glucose-methanol-choline oxidases) superfamily of oxidoreductases [5]. One of the similarities with some of these FAD-containing enzymes is the presence of two conserved histidines involved in catalysis, His^{502} and His^{546} in *Pleurotus eryngii* AAO. The importance of these AAO histidines in the enzymatic process has been shown by mutational studies [6]. The crystal structure for *P. eryngii* AAO (PDB entry 3FIM) has recently been obtained [7] confirming the catalytically relevant position of His^{502} and His^{546}, right in the vicinity of the FAD cofactor (Figure 1, left) and the structural relationship of AAO with choline oxidase (CHO). One of the questions that arise from the inspection of the crystal structure is the entrance of large ligands into the active site. The structure does not present an obvious entrance channel and the packing in the active site appears quite compact. In particular, Tyr^{92} blocks the access to the catalytic N5 of the isoalloxazine ring of AAO FAD, requiring large residue reorganization upon ligand entrance.

In the GMC superfamily, the most accepted catalytic mechanism starts with a proton abstraction from alcohol substrate by an active site base, which could correspond to the above-mentioned His^{502} or His^{546} in *P. eryngii* AAO and to His^{466} (or His^{351}) in *Arthrobacter globiformis* CHO (Figure 1), followed by hydride transfer to the FAD N5. The process continues by O_2 reduction to H_2O_2 by FAD. Mechanistic studies based on substrate kinetic isotope effects (KIE) in CHO and methanol oxidase proposed the existence of two distinct steps in the reductive half-reaction, with the rate limiting step being the hydride transfer from a protein-stabilized substrate alkoxide [8;9]. Mutational studies on CHO [10-12] have aimed to address the role of the active site residues in the catalytic process. Both His^{466} and His^{351} are important for the alcohol proton abstraction, although there is not a clear picture of the identity of the base; additionally, Glu^{312} appears to be important for the substrate binding by CHO.

Computer simulations, mechanistic and site-directed mutagenesis experiments have been used here to investigate the structural basis for the migration of *p*-anisyl alcohol, the natural AAO substrate [13], and 2,4-hexadien-1-ol, a structurally different AAO substrate [1], into the active site, and the hydride (and proton) transfer reaction during catalysis. For the sake of comparison, simulations of choline oxidation by the related CHO are also presented. Ligand migration and induced fit were simulated with PELE [14], a recently developed methodology capable of modelling protein-ligand recognition mechanisms. To obtain a description of the oxidation mechanism, we used mixed quantum mechanics and molecular mechanics (QM/MM) methods that combine a classical region, described by a set of "solid" spheres with point charges and classical force fields, with a quantum region where the Schrödinger equation is solved. Thus, the explicit electronic description of the system is limited to the QM region covering all the atoms involved in the biochemical process [15;16].

MATERIALS AND METHODS

Enzyme and mutated variants

Recombinant AAO of *P. eryngii* was obtained by *Escherichia coli* expression of the mature AAO cDNA (GenBank™ AF064069) followed by *in vitro* activation [17]. AAO variants were prepared using the QuikChange site-directed mutagenesis kit (Stratagene). For the PCR reactions, the AAO cDNA cloned into the pFLAG1 vector was used as template, together with oligonucleotides bearing the required mutations (see Supplementary section S1.1). Mutations were confirmed by sequencing (GS-FLX sequencer from Roche) and the mutated variants were produced [17]. Enzyme concentrations were determined using molar absorbances: AAO, ε_{463} 11050 $M^{-1}\cdot cm^{-1}$; H502S, ε_{468} 9980 $M^{-1}\cdot cm^{-1}$; H502A, ε_{467} 9800 $M^{-1}\cdot cm^{-1}$; H546S ε_{463} 12400 $M^{-1}\cdot cm^{-1}$; and H546A, ε_{467} 9669 $M^{-1}\cdot cm^{-1}$.

Steady-state and transient-state kinetic measurements

Enzyme activity under steady-state conditions was monitored spectrophotometrically by linear-phase oxidation of *p*-anisyl alcohol (from Sigma-Aldrich) to *p*-anisaldehyde (ε_{285} 16950 $M^{-1}\cdot cm^{-1}$) [1]. Kinetic constants were determined varying simultaneously the concentration of *p*-anisyl alcohol and O_2 in 0.1 M phosphate, pH 6, at 25 ºC, for the wild-type AAO, H546S and H546A variants (for details see Supplementary section S1.2). For the H502S and H502A variants, the steady-state constants were determined only varying the alcohol concentration under air-saturated buffer, since the (low) enzyme turnover rates were independent from O_2 concentration, and the constants were obtained by fitting the initial rate data to the Michaelis-Menten equation. pH dependence of steady-state kinetic constants in AAO mutated variants was studied at 25 ºC in air-saturated 0.1 M citrate phosphate for pH 3–7, and 0.1 M pyrophosphate for pH 8–9 (for the equations used see Suplementary section S1.3). For transient-state kinetic studies, an Applied Photophysics SX18.MV stopped-flow spectrophotometer, interfaced with an Acorn computer, was used (together with the SX18.MV and Xscan softwares). Reductive half-reactions were analysed under anaerobic conditions [18] at different temperatures, and analyses were performed using the Pro-K software (Applied Photophysics) (see Supplementary section S1.4).

AAO and CHO model setup

AAO computational studies were based on the crystal structure 3FIM [7]. After visual inspection, histidines 91, 313, 387 and 398 were protonated in its ε position (Hie), and histidines 137, 148 and 360 were protonated in both its ε and δ positions (Hip, positively charged); all other histidines were δ protonated (Hid). The protonation state of the catalytically-active histidines, His^{502} and His^{546}, were further studied with molecular dynamics (MD) and QM/MM methods.

For CHO we started from the 2JBV A-chain holo crystal structure [11]. The side-chains of Glu^{222} and Glu^{340} were completed and sampled with PLOP [19]. The oxygen atom forming an adduct with the FAD cofactor [20] was removed and the crystal substrate analogue, dimethylsulphoxide, was used to model the cognate choline substrate. After visual inspection histidines 310, 506, 257 and 148 were protonated in its ε position and histidines 216 and 149 were protonated in both its ε and δ positions; all other histidines were δ protonated. Due to the presence of the dimethylsulphoxide molecule, it was not necessary to diffuse the ligand into the active site, as described for AAO. The system was then equilibrated with a 1 ns MD trajectory. After the initial 200 ps in the MD trajectory, the choline substrate adopted a catalytic position, where the alcohol group was in close contact with His^{466}.

Ligand and protein dynamic exploration: PELE

The Protein Energy Landscape Exploration (PELE) algorithm combines a steered stochastic approach with protein structure prediction methods, capable of projecting the migration dynamics of ligands in proteins [14;21;22]. PELE's heuristic algorithm is based on three main steps: **i)** Ligand and protein local perturbation, including translation and rotation of the ligand, and protein α-carbon displacement following an anisotropic network model approach; **ii)** Side-chain sampling, by placing all side-chains local to the ligand; and **iii)** Energy minimization, involving the minimization of a region including, at least, all residues local to the atoms involved in **i** and **ii**. Typically, a simulation involves several processors running multiple steps and sharing information towards addressing a common task. SiteMap [23] was used for exploring cavities in AAO, and localizing the start point for PELE migrations.

Protonation predictors and MD calculations

Three programs were used to calculate theoretical hydrogen positions and pK_a values of the putative bases: i) WhatIf [24], which uses hydrogen bonding patterns to choose the best protonation state of titratable residues; ii) Adaptive Poisson Boltzmann Solver (APBS) [25] to calculate intrinsic pK_a shifts by the surrounding residues in single snapshots using the Poisson-Boltzmann equation; and iii) Interaction Cluster Decomposition Algorithm (ICDA) [26], which

uses rotamer library sampling of clusters of titratable residues scored with a molecular mechanics force field and generalized Born implicit solvation

MD calculations were performed with the NAMD version 2.6 [27] starting from structures provided by the previous ligand migration. The proteins were solvated in a 0.5 M NaCl solution in periodic boxes of 90 x 80 x 70 Å. Each system contained approximately 12000 water molecules and 46000 total atoms, and was equilibrated by a minimization followed by 10 ps of MD in the NVT ensemble followed by 0.5 ns each in the NPT and NVT ensembles with a step size of 1 fs. Production runs consisted of 5 ns of MD with a 2 fs step size in the NVT ensemble using the particle mesh Ewald method to treat long-range electrostatics.

QM/MM and QM Calculations

All QM/MM calculations were performed with the Qsite program [28] using the density functional theory (DFT) B3LYP level of theory, the 6-31G* basis set, and the hydrogen like boundary approximation. Unless noted, the quantum region included: the flavin, the ligand (alcohol substrate), the three active site histidines (502, 313 and 546 in AAO and 466, 310 and 351 in CHO), Glu^{389} in AAO and Gln^{510} in CHO. The OPLS-AA force field was used for the treatment of the molecular mechanism part, with 100 Å non bonding cuttoff. For both enzymes the QM/MM initial system was obtained after equilibration of an explicit water system with MD and by removing all water molecules beyond 10 Å from the protein surface. All geometry optimizations were performed by harmonically constraining the oxygen atom of the outermost 5 Å of the water layer (beyond 20 Å of any atom in the QM region). Gas phase second-order Moller Plesset (MP2) QM calculations were performed using Gaussian03 [29] with a 6-311G* basis set.

The QM region size (~160 atoms) and methodology (B3LYP) does not allow us to go beyond a QM/MM reaction coordinate analysis (geometry optimizations along a proton/hydride reaction coordinate). This same level of theory, however, has shown very good agreement in many enzymatic systems [15;16]. When building the QM/MM reaction coordinates, the possibility of a proton transfer followed by a hydride transfer and the reverse process have been considered. The x axis is the sum of the proton and hydride transfer distances (proton to proton-acceptor distance); large values corresponding to the alcohol reactants and smaller ones to the aldehyde products. For each protonation state (see below) we studied three different mechanisms. The first two involve only one transferred atom being forced to move (either the proton or the hydride) with 0.15 Á increments. The donor-transferred distance is then constrained and the rest of the system is minimized. The third mechanism involves the simultaneous (concerted) movement of both atoms.

RESULTS

Computational and experimental studies were combined to unravel the mechanism of alcohol oxidation at the buried active site of AAO. First, the alcohol migration pathway from the protein surface was determined using the PELE software after cavity exploration. Then, the role of two active-site histidines was experimentally investigated by site-directed mutagenesis, and their protonation states predicted with the purpose of identifying the catalytic base. Finally, energy profiles of the reactions of AAO, and related CHO, were obtained by QM/MM methods to determine the timing of the proton and hydride transfers, and the existence of reaction intermediates.

Ligand migration to the AAO active site

In the AAO crystal structure, the buried active site has only few water molecules, without a large cavity and with the access to the catalytic N5 of the FAD blocked by Tyr^{92} and other residues (Figure 1, left). Thus, direct docking of large ligands, such as AAO aromatic alcohol substrates, does not seem an appropriate procedure. This was confirmed when exploring possible cavities

with SiteMap, which could only find binding sites on the protein surface. Thus, we proceed to dock the ligand on the surface for subsequent migration into the active site by PELE. Interestingly, the highest score surface lies in the vicinity of Pro^{402}, next to a flexible loop that connects the surface and the active site. To better characterize the migration entrance, we mutated *in silico* the active site water molecule shown in Figure 1 into methanol and performed migration simulations by passing to PELE the task of moving the ligand away from its initial position, with random non preassigned directions. After 3 simulations with different Metropolis temperatures (300, 500 and 1000 K) all simulations resulted in the same exit pathway, ending in the SiteMap best scoring surface cavity (Supplementary Figure S1).

The agreement between the surface cavity finder and the methanol expulsion migration clearly points to the entrance of the ligand migration channel. We placed the *p*-anisyl alcohol and 2,4-hexadien-1-ol ligands at this surface point and ask PELE to migrate them towards the active site by setting a common task of shortening the distance with His^{502}, whose role in catalysis is discussed below. Figure 2 shows the energy profile for this diffusion to the active site for the 2,4-hexadien-1-ol ligand, which was equivalent to the *p*-anisyl alcohol energy profile. The internal energy of hundreds of conformations is plotted against the ligand-FAD distance, and three minima are clearly observed. The energy profile indicates that the entrance is located at a distance of ~17 Å from the isoalloxazine ring, next to Pro^{402}. From this point the motion of the ligand is highly coupled to oscillations of the Gln^{395}-Thr^{406} loop. The second minimum corresponds to the first stable intermediate at ~11 Å from the isoalloxazine ring of FAD, where it interacts (through π interaction) with Phe^{397}. At this stage, further migration of the ligand to the active site requires side-chain readjustment of this phenylalanine residue, of several hydrophobic residues (such as Leu^{315} and Ile^{391}) and of Tyr^{92}. In the active site, the ligands adopt catalytically-active conformations at distances of ~5 Å (ligand center of mass to N5) from the isoalloxazine ring.

Figure 3 shows three snapshots along the *p*-anisyl alcohol migration pathway corresponding to the three energy minima shown in Figure 2. On the left panel we show a representative conformation for the surface docked structure. On the middle panel we show the intermediate where we clearly observe the π-π stacking between the substrate *p*-anisyl alcohol and Phe^{397}. The right panel indicates an active-site conformation, where we underline the proton and hydride abstraction coordinates with pink lines. This last structure corresponds to the catalytically-active species from which we performed the QM/MM and other calculations described below.

The latter structure also suggests that Tyr^{92} at the active site would establish π-π stacking interactions with the alcohol substrate. The interaction observed is not a parallel stacking interaction, but an edge-to-face (T-shaped) interaction (Figure 3C). Quantum mechanics Moller Plesset (MP2) interaction energies, at the final geometries obtained with PELE, confirmed the nature of these stacking interactions. We obtained -2.7 and -1.6 kcal.mol^{-1} stabilization energies for the *p*-anisyl and 2,4-hexadien-1-ol alcohols, respectively.

Additionally, three movies were produced to illustrate the ligand migration into the active site (Supplementary Movies S1-S3).

Mutagenesis of active site histidines: Kinetic parameters and pH profiles

In addition to the above tyrosine residue involved in substrate stabilization, the AAO active site also includes two conserved histidines (Figure 1). Using site-directed mutagenesis, we experimentally replaced these two histidines by serine and alanine residues in the H502S/A and H546S/A independent variants. The two H502S/A variants showed a strong turnover decrease (around 2900 folds), while the H546S/A mutations caused milder decreases (12 and 60-fold, respectively) (Table 1). All the substitutions also caused an increase in the K_m for the alcohol substrate, which was higher for the H502S/A (27 and 80-fold increases, respectively) than for the H546S/A (8 and 25-fold increases, respectively) variants. The above changes made the H546S, H546A, H502S and H502A variants, respectively, 80, 1450, 80000 and over 200000 folds less efficient than wild-type AAO oxidizing *p*-anisyl alcohol.

The reductive (substrate oxidation) half-reactions of the H502S/A and H546A variants were further investigated under anaerobic conditions using stopped-flow spectrophotometry (the low stability of H546S prevented this characterization). As previously found for AAO, no intermediates were detected during flavin reduction to the hydroquinone state in these variants. The observed rate constants showed hyperbolic dependence on the *p*-anisyl alcohol concentration, allowing determination of AAO reduction (k_{red}) and substrate dissociation (K_d) constants (Table 1). The k_{red} values for the H546A, H502S, H502A and variants were at least 35, 1200 and 1800-fold lower, respectively, than those of the wild-type AAO, and a strong decrease of the alcohol affinity (50-200 fold higher K_d values) was also observed. All together these data confirm that both His^{502} and His^{546} participate in AAO catalysis, playing a crucial role during the reductive-half reaction.

Wild-type AAO does not show a clear pH dependence for oxidation of *p*-anisyl alcohol and other alcohol substrates. However, replacement of His^{546} resulted in a clear effect of pH in the oxidation of *p*-anisyl alcohol (Figure 4). The catalytic efficiency profile of H546S showed a residue in the free enzyme with an apparent pK_a value of 3.8 that must be unprotonated for catalysis. The effect of pH on the variant turnover resulted in a bell-shaped profile, consistent with the involvement of two ionizable groups in the substrate-binding site. One group with a pK_a $\leq$3.5 must be unprotonated for activity, and one with a pK_a $\geq$8.3 must be protonated. As shown in Table 1, the activity of the H502S and H502A variants was extremely low, hampering catalytic efficiency estimation under different pH conditions. However, a pK_a $\geq$7.5 could be determined for the H502S turnover (Figure 4B). It corresponds to a residue that must be protonated during turnover at the same time that the previously observed pK_a $\leq$3.5 disappeared suggesting that it corresponds to the His^{502} removed in the present variant.

Protonation states of His^{502}, His^{546} and other active site residues

The mutational studies indicate the importance of His^{502} and His^{546} in catalysis, but do not reveal whether they are protonated at the δ/ε positions (Hid/Hie) or at both positions (Hip), a central aspect to identify the catalytic base. We have studied the protonation state of the Glu^{389}/His^{546}/His^{502}/His^{313} cluster with three different predictors. With the alcohol substrate present, all these methods agreed that the net charge of the cluster should be zero with the differences being which residue should be preferentially protonated. WhatIF and ICDA protonate Glu^{389} whereas APBS protonates His^{546}. Thus, as expected, the negative charge of Glu^{389} in the active site is screened, although it is not clear who carries the proton.

To determine more accurately which of these would be protonated a QM/MM minimization was performed on the substrate-free crystal structure with the three histidines, the glutamic acid and the flavin included as the QM region. When His^{546} was protonated (Hip^{546}), a spontaneous proton transfer occurred between His^{546} and Glu^{389}, forming a neutral glutamic, Glh^{389}, and reducing the charge separation in the active site. When His^{313} or His^{502} were protonated (to give Hip^{313} or Hip^{502}), it resulted in a less stable conformation (+8.9 and +2.5 kcal·mol^{-1}, respectively) than His^{546} being protonated. The heavy-atom RMSD to the crystal structure was also smaller when Hip^{546} was protonated (0.63 Å) confirming that the final state, with the neutral Glu^{389}, is the correct starting configuration. The same results were obtained with *p*-anisyl alcohol bound. The neutral nature of Glu^{389} agrees with its buried hydrophobic environment in the crystal structure. This is in contrast with the equivalent glutamic acid in CHO, Glu^{312}, which is in contact with a large water cluster in the crystal structure. APBS, for example, gives a pK_a for Glu^{389} of 8.19 (similar to the highest pK_a experimentally obtained for the AAO histidine variants, Figure 4B) corresponding to a residue that should be protonated for catalysis) whereas we obtain a value of 5.4 for the Glu^{312} in CHO.

To further explore the possible combinations between His^{502} and His^{546}, we performed 5 ns MD for 6 different protonation states: His^{546} in three possible protonation states (Hid, Hie and Hip) and two possible protonation states for His^{502} (Hid and Hie). The results show that only the combination of Hip^{546} and Hid^{502} produced a stable catalytic species where both the proton

abstraction (by the histidine base) and the hydride transfer (to flavin N5) distances were simultaneously optimal (see Supplementary section S2.2 and Figure S2). To illustrate the situation, Figure 5A and B indicates the initial and final states when His^{546} is protonated, which is favoured by the QM/MM and MD simulations, and Figure 5C indicates the Hie^{502}/Hie^{546} protonation state.

QM/MM analysis of the AAO and CHO enzymatic reactions

From the catalytically-active species produced after ligand migration, we proceed to compute the QM/MM energy profile for the alcohol oxidation. Previous analyses have indicated that the $Glh^{389}/Hid^{502}/Hid^{546}$ state is preferred to the Hie^{502}/Hie^{546} one (Figure 5B and C, respectively). We have built, however, the oxidation energy profiles for both cases, which were labelled as Glh^{389}/Hid^{502} and Hie^{502}/Hie^{546}. In the first case, His^{502} accepts the proton and His^{546} hydrogen bonds the oxygen alcohol. For the Hie^{502}/Hie^{546} case the roles are inverted.

Figure 6A shows the energy profile obtained for these two protonation states for *p*-anisyl alcohol. As expected in these types of reaction mechanism, the profiles indicate that the proton is the first to be transferred; starting the process with the hydride results in larger (and earlier) energy barriers. In all cases, the main component of the energy barrier corresponds to the hydride transfer. Figure 6B shows the corresponding energy profiles for the 2,4-hexadien-1-ol oxidation. We plot the energy profiles where the proton is being transferred first since the hydride first mechanism gave identical results as in the *p*-anisyl case. The third mechanism explored, the concerted-synchronous transfer with simultaneous transfer of the proton and hydride, introduce higher barriers for both substrates. All attempts to locate a transition state for the synchronous transfer in any of the substrates resulted in barriers above 30 kcal·mol^{-1}.

In the Hie^{502}/Hie^{546} case (Figure 5C) transferring the proton to Hie^{546} involves a second spontaneous proton transfer event to Glu^{389} in both 2,4-hexadien-1-ol and *p*-anisyl alcohol. Therefore, the glutamate side-chain acts as the final base, in agreement with the previous protonation and pK_a calculations. In the Glh^{389}/Hid^{502} case (Figure 5B), His^{502} is hydrogen bonded to another histidine, His^{313}, which could act as the final base. However, all attempts to expand the proton relay to His^{313}, before and after the hydride transfer and for both substrates, resulted in non stable structures, the proton being transferred back to His^{502}.

The crystal structure in CHO indicates a correlation between His^{466} and AAO His^{502}, while the position of AAO His^{546} is occupied by an asparagine in CHO (Figure 1). There is, however, a second histidine in CHO capable of acting as a base, His^{351}. We have tried four different possibilities for the base in CHO using QM/MM: His^{351}, His^{466}, Glu^{312}, and the flavin O4. Only when using His^{466} as a base we obtained a low barrier energy profile with a stable alkoxide intermediate. Using flavin O4 as base results in a profile with ~40 kcal energy increase. Analogous to His^{546} in AAO, abstraction of a proton from His^{351} induces a spontaneous transfer from the histidine to Glu^{312}. Thus, the final state is the same when using His^{351} or Glu^{312} as a base. The energy profile indicates a barrier of ~20 kcal·mol^{-1} and endothermicity of 18 kcal·mol^{-1}, which translates into a non stable alkoxide intermediate.

Figure 7 compares the CHO and AAO energy profiles when using His^{466} and His^{502} as bases, respectively. CHO oxidation presents a low energy barrier, ~10 kcal·mol^{-1}, and has a stable intermediate as a result of the first proton transfer event, ~6 kcal·mol^{-1} higher than the reactants, while no intermediate is stabilized in the AAO reaction. Moreover, in contrast with that observed in AAO, the alcohol proton abstraction in CHO drives a second spontaneous proton transfer from His^{466} to His^{310} (Figure 1). The second proton transfer results in ~3 kcal·mol^{-1} relaxation, being a significant part of the intermediate stabilization in CHO. As seen in Figure 7, the energy profile for the second part of the process, the hydride transfer, is almost identical in both systems; the exothermicity of the process in CHO comes mainly from the intermediate stabilization.

DISCUSSION

Substrate diffusion to reach the buried active site of AAO

The simulations on ligand binding and migration clearly indicate that the alcohol substrate entrance into the active site of AAO is highly coupled to oscillations of the Gln^{395}-Thr^{406} loop. As recently reported [7], this loop represents a characteristic structural feature of AAO crystal structure, when compared with glucose oxidase and CHO structures. Although its active site entrance is considerably more open, due to the absence of the loop, a gating mechanism has recently been proposed in CHO [30].

The energy profile shows the existence of an intermediate along the PELE migration pathway, where the AAO ligand interacts with Phe^{397}. Ligand entrance coupled to phenylalanine motions seems to be a common feature and has been recently observed in several systems such as cytochrome P450cam [14;31]. Once in the active site, the ligand adopts easily a catalytic position, with the alcohol hydrogen pointing to the possible histidine bases, and one of the α-hydrogens to the FAD N5 for hydride transfer (at 2.4-2.5 Å distances) by means of a π-π interaction with Tyr^{92}. Our studies suggested that the latter is a T-shaped interaction. T-shaped stacking interactions have been largely characterized in biological systems [32] being also one of the main local minima in the benzene dimer [33]. Reported mutations of AAO Tyr^{92} [6] have shown that an aromatic residue is required at this position, the Y92A variant being inactive but the Y92F variant maintaining basically the same kinetic parameters of the wild-type enzyme, supporting the involvement of the above π-π interaction in AAO catalysis.

Concerted non-synchronous mechanism for alcohol oxidation by AAO

The role of conserved active-site histidines as putative catalytic bases and acids for the reductive and oxidative half-reactions, respectively, has been extensively discussed in the GMC superfamily [8;34-36].

Our mutational studies indicate the importance of the two AAO histidines in the first step of the redox process (i.e. the reductive half-reaction). His^{546} seems to play a similar role in substrate binding and oxidation, as revealed by 20-60 fold decreases in k_{cat} and k_{red}, and similar increases in alcohol K_m and K_d, for the H546A variant. This role of His^{546} on substrate stabilization agrees with the molecular mechanic studies. The Hid^{502}/Hip^{546} protonation state produces the best alignment for the ligand catalysis, with optimal proton and hydride transfer distance. Inspection of the crystal structure, with His^{546} lying next to Glu^{389}, seems to indicate the positive nature of the former residue (or the protonation of Glu^{389}). The protonation studies further agree with this visual inspection: Glu^{389} is protonated, with His^{546} and His^{502} being neutral and with δ protonation. Thus, in the wild-type enzyme, we would expect His^{502} to act as the base, in agreement with the mutational studies showing around 3000-fold decrease in k_{cat}, and at least 1000-fold decrease in k_{red}, after its substitution by alanine or serine. It is necessary to mention that, in addition to its main role as the catalytic base, an effect on substrate binding is also exerted by His^{502}, resulting in lower affinity (27-80 fold higher alcohol K_m, and 100-200 fold higher K_d) in the above variants. Mutations that might open the AAO active site or change its polarization, decreasing Glu^{389} pK_a, would open the possibility of using His^{546} as a base.

The AAO QM/MM energy profiles indicate the presence of very weak (with a ~1-2 kcal·mol^{-1} barrier back to the reactants) intermediates in alcohol oxidation. The calculations provide only internal energies, not including vibration zero-point nor thermal energies. Corrections for these energies are on the order of 3-4 kcal/mol for a proton transfer reaction [37-39] (see, for example Figure 3 in [37]). Thus, including these effects all energy profiles will present no intermediates, indicating a concerted mechanism for the proton and hydride transfers in AAO catalysis. This is in agreement with mechanistic studies using α-dideuterated *p*-anisyl alcohol and 2,4-hexadien-1-ol as substrates and deuterium oxide as reaction solvent [40]. The former revealed a strong substrate kinetic effect, and supported the hydride transfer mechanism in AAO, while the latter showed the existence of a low but consistent solvent KIE (and clear multiple KIE when both deuterated substrate and solvent were combined) for AAO oxidation of alcohol substrates (Table 2). These KIE were observed under both steady-state and transient-state conditions, and were

indicative of a concerted proton and hydride transfer mechanism. A similar concerted proton and hydride transfer mechanism has been recently reported for AAO oxidation of some aromatic aldehydes bearing electron-withdrawing substituents, which promote formation of the *gem*-diol substrates [41]. A concerted mechanism occurs in a single step, but it does not tell anything of the synchronous or non-synchronous bond breaking. We have investigated both mechanisms for alcohol oxidation by AAO and any attempt to locate a synchronous proton and hydride transfer resulted in very large barriers, while the non-synchronous mechanism was significantly lower in energy. Non-synchronous concerted oxidation mechanisms, as described here for AAO, have been reported for other oxidoreductases [42].

Catalytic mechanisms in GMC oxidoreductases: A comparison between CHO and AAO

During recent years, the catalytic mechanism of CHO has been investigated in detail as a model GMC oxidoreductase [8]. In CHO the active site polarity changes significantly with respect to AAO. The pK_a analysis of its active site glutamic acid, Glu^{312}, reveals an anionic side-chain at physiological pH. Mutation of Glu^{312} causes a 500-fold increase in the K_d value [11]. Thus, it seems clear that this glutamic acid remains negative for an effective interaction with the trimethylammonium group of choline.

When comparing the CHO QM/MM energy profiles we obtain His^{466} as the main base (in both AAO and CHO the histidine in front of the flavin appears as the base). The reduction in pK_a for Glu^{312}, compared to that for Glu^{389} in AAO, drastically increases the energy barrier and intermediate energies for the second histidine path in CHO, the His^{351}-Glu^{312} path. While the studies of Gadda and co-workers [10;12] have not definitively concluded the nature of the CHO base, mutation of His^{466} has the larger effect on k_{cat}. More recently, Gadda [8] suggested that either one of the active site histidines in CHO (His^{351} and His^{466}) act as the base (being replaced by the second histidine when mutated) or, alternatively, the acidification of the substrate hydroxyl and proton loss to the solvent may occur through interactions with multiple active-site residues. However, the observation of a two step kinetic process in CHO, and the existence of a stable intermediate in the QM/MM energy profiles obtained in the present study, suggest His^{466} being the base in CHO. H466A mutation drastically reduces k_{cat} and eliminates the two step process [8;10] which would be consistent with the activation of the His^{351}-Glu^{312} path, with a proton abstraction energy barriers equivalent to that of the hydride transfer.

One of the main differences between CHO and AAO is the presence of a stable intermediate for the initial proton transfer in CHO. This intermediate is partially the result of a proton relay involving His^{466} and His^{310}. The same mechanism could be operative in AAO due to the presence of His^{313}. However, our calculations indicate that in AAO this second proton transfer does not occur. The local environment of this second histidine is significantly different in both enzymes. In CHO, His^{310} is in closer interaction with two carbonyl groups, from Val^{507} and Thr^{380}, and its side-chain forms a stacking interaction with another histidine side-chain, His^{506}. Thus, the proton relay in CHO seems more favourable due to the electrostatic stabilization of the two carbonyl groups and the π-cation interaction with His^{506}. The existence of a stable intermediate in the proton transfer in CHO agrees with the observations of a two step process for this enzyme, as opposed to the concerted mechanism observed in AAO. The existence of these divergent mechanisms is in agreement with the absence of a solvent KIE in choline oxidation by CHO investigated under both steady-state and transient state conditions [43;44], while a solvent effect was observed for AAO oxidation of the two alcohols investigated here [40] (Table 2). The non-synchronous concerted mechanism for alcohol oxidation by AAO, based on both the KIE results and QM/MM energy profiles, would be different from the sequential mechanism proposed for CHO and other GMC oxidoreductases [8;43].

Conclusions

Using experimental and computational techniques we have studied the ligand diffusion and oxidation processes in AAO, compared with CHO. We find that the substrate entrance is next to

the Gln[395]-Thr[406] loop, bypassing and interacting with Phe[397] and, once in the active site, side-chain readjustment is required for a stacking interaction with Tyr[92]. QM/MM and site-directed mutagenesis results show that His[502] and His[546] are involved in catalysis, their substitution strongly decreasing both k_{cat} and k_{red}. The theoretical energy profiles, protonation predictors, and mutagenesis studies give a robust answer about the nature of the catalytic base: the histidine residue directly in front of the FAD cofactor ring (AAO His[502], corresponding to CHO His[466]) acts as the base. Furthermore, for the two substrates assayed, it was shown that proton transfer preceded hydride transfer, although both processes are highly coupled. In AAO the QM/MM energies do not find a stable intermediate along the proton and hydride transfer coordinates. In CHO, however, we find a stable intermediate after proton abstraction, in line with previous findings. The atomic resolution of the computational analysis allows us to narrow down these differences with changes in the active site. Overall the combination of theoretical and solvent KIE studies, suggest a non-synchronous concerted mechanism for alcohol oxidation by AAO.

Author contributions

Aitor Hernández-Ortega, Patricia Ferreira, Milagros Medina and Angel T. Martínez contributed with the experimental part of the work, and Kenneth Borrelli and Victor Guallar contributed with the computational part. Although all the authors participated in the interpretation and discussion of results, Victor Guallar, Angel T. Martínez and Milagros Medina especially contributed to integrate the two parts of the study.

Acknowledgments

The authors thank the Barcelona Supercomputing Center for computational resources. A.H.-O. thanks a predoctoral contract from the Comunidad de Madrid, and P.F. thanks a Juan de la Cierva contract of the Spanish Ministry of Science and Innovation.

Funding

This work was supported by the Spanish Ministries of Education and Science, through the project CTQ2007-62122 (to V.G.), and Science and Innovation, through the projects BIO2010-1493 (to M.M.) and BIO2008-01533 (to A.T.M.); and by the EU, through the NMP2-CT-2006-026456 (BIORENEW) and KBBE-2010-4-265397 (PEROXICATS) projects (to A.T.M.).

REFERENCES

1 Ferreira, P., Medina, M., Guillén, F., Martínez, M. J., van Berkel, W. J. H. and Martínez, A. T. (2005) Spectral and catalytic properties of aryl-alcohol oxidase, a fungal flavoenzyme acting on polyunsaturated alcohols. Biochem.J., **389,** 731-738

2 Ruiz-Dueñas, F. J. and Martínez, A. T. (2009) Microbial degradation of lignin: How a bulky recalcitrant polymer is efficiently recycled in nature and how we can take advantage of this. Microbial Biotechnol., **2,** 164-177

3 Martínez, A. T., Ruiz-Dueñas, F. J., Martínez, M. J., del Río, J. C. and Gutiérrez, A. (2009) Enzymatic delignification of plant cell wall: from nature to mill. Curr.Opin.Biotechnol., **20,** 348-357

4 Varela, E., Martínez, A. T. and Martínez, M. J. (1999) Molecular cloning of aryl-alcohol oxidase from *Pleurotus eryngii*, an enzyme involved in lignin degradation. Biochem.J., **341,** 113-117

5 Varela, E., Martínez, M. J. and Martínez, A. T. (2000) Aryl-alcohol oxidase protein sequence: A comparison with glucose oxidase and other FAD oxidoreductases. Biochim.Biophys.Acta, **1481,** 202-208

6 Ferreira, P., Ruiz-Dueñas, F. J., Martínez, M. J., van Berkel, W. J. H. and Martínez, A. T. (2006) Site-directed mutagenesis of selected residues at the active site of aryl-alcohol oxidase, an H_2O_2-producing enzyme. FEBS J., **273,** 4878-4888

7 Fernández, I. S., Ruiz-Dueñas, F. J., Santillana, E., Ferreira, P., Martínez, M. J., Martínez, A. T. and Romero, A. (2009) Novel structural features in the GMC family of oxidoreductases revealed by the crystal structure of fungal aryl-alcohol oxidase. Acta Crystallogr.D.Biol.Crystallogr., **65,** 1196-1205

8 Gadda, G. (2008) Hydride transfer made easy in the reaction of alcohol oxidation catalyzed by flavin-dependent oxidases. Biochemistry, **47,** 13745-13753

9 Menon, V., Hsieh, C. T. and Fitzpatrick, P. F. (1995) Substituted alcohols as mechanistic probes of alcohol oxidase. Bioorg.Chem., **23,** 42-53

10 Ghanem, M. and Gadda, G. (2005) On the catalytic role of the conserved active site residue His466 of choline

oxidase. Biochemistry, **44,** 893-904
11 Quaye, O., Lountos, G. T., Fan, F., Orville, A. M. and Gadda, G. (2008) Role of Glu312 in binding and positioning of the substrate for the hydride transfer reaction in choline oxidase. Biochemistry, **47,** 243-256
12 Rungsrisuriyachai, K. and Gadda, G. (2008) On the role of histidine 351 in the reaction of alcohol oxidation catalyzed by choline oxidase. Biochemistry, **47,** 6762-6769
13 Gutiérrez, A., Caramelo, L., Prieto, A., Martínez, M. J. and Martínez, A. T. (1994) Anisaldehyde production and aryl-alcohol oxidase and dehydrogenase activities in ligninolytic fungi from the genus *Pleurotus*. Appl.Environ.Microbiol., **60,** 1783-1788
14 Borrelli, K. W., Vitalis, A., Alcantara, R. and Guallar, V. (2005) PELE: Protein energy landscape exploration. A novel Monte Carlo based technique. J.Chem.Theory Comput, **1,** 1304-1311
15 Senn, H. M. and Thiel, W. (2007) QM/MM methods for biological systems. Atomistic Approaches in Modern Biology: from Quantum Chemistry to Molecular Simulations, **268,** 173-290
16 Friesner, R. A. and Guallar, V. (2005) Ab initio quantum chemical and mixed quantum mechanics/molecular mechanics (QM/MM) methods for studying enzymatic catalysis. Annu.Rev.Phys.Chem., **56,** 389-427
17 Ruiz-Dueñas, F. J., Ferreira, P., Martínez, M. J. and Martínez, A. T. (2006) In vitro activation, purification, and characterization of *Escherichia coli* expressed aryl-alcohol oxidase, a unique H_2O_2-producing enzyme. Protein Expr.Purif., **45,** 191-199
18 Fraaije, M. W. and van Berkel, W. J. H. (1997) Catalytic mechanisms of the oxidative demethoxylation of 4-(methoxymethyl)phenol by vanillyl-alcohol oxidase. Evidence for formation of a *p*-quinone methide intermediate. J.Biol.Chem., **272,** 18111-18116
19 Jacobson, M. P., Pincus, D. L., Rapp, C. S., Day, T. J. F., Honig, B., Shaw, D. E. and Friesner, R. A. (2004) A hierarchical approach to all-atom protein loop prediction. Proteins, **55,** 351-367
20 Orville, A. M., Lountos, G. T., Finnegan, S., Gadda, G. and Prabhakar, R. (2009) Crystallographic, spectroscopic, and computational analysis of a flavin C4a-oxygen adduct in choline oxidase. Biochemistry, **48,** 720-728
21 Guallar, V., Lu, C. Y., Borrelli, K., Egawa, T. Y. and Yeh, S. R. (2009) Ligand migration in the truncated hemoglobin-II from *Mycobacterium tuberculosis*: The role of G8 tryptophan. J.Biol.Chem., **284,** 3106-3116
22 Borrelli, K., Cossins, B. and Guallar, V. (2010) Exploring hierarchical refinement techniques for induced fit docking with protein and ligand flexibility. J.Comp.Chem., **31,** 1224-1235
23 Halgren, T. (2007) New method for fast and accurate binding-site identification and analysis. Chem.Biol.Drug Design, **69,** 146-148
24 Vriend, G. (1990) WHAT IF: A molecular modeling and drug design program. J.Mol.Graph., **8,** 52-56
25 Baker, N. A., Sept, D., Joseph, S., Holst, M. J. and McCammon, J. A. (2001) Electrostatics of nanosystems: Application to microtubules and the ribosome. Proc.Natl.Acad.Sci.USA, **98,** 10037-10041
26 Li, X., Jacobson, M. P., Zhu, K., Zhao, S. and Friesner, R. A. (2007) Assignment of polar states for protein amino acid residues using an interaction cluster decomposition algorithm and its application to high resolution protein structure modeling. Proteins, **66,** 824-837
27 Phillips, J. C., Braun, R., Wang, W., Gumbart, J., Tajkhorshid, E., Villa, E., Chipot, C., Skeel, R. D., Kale, L. and Schulten, K. (2005) Scalable molecular dynamics with NAMD. J.Comput.Chem., **26,** 1781-1802
28 Schrödinger Inc. (2007) QSite 4.5, Schrödinger, Inc., Portland, Oregon
29 Frisch, M. J., Trucks, G. W., Schlegel, H. B., Scuseria, G. E., Robb, M. A., Cheeseman, J. R., Montgomery, J. J. A., Vreven, T., Kudin, K. N., Burant, J. C., Millam, J. M., Iyengar, S. S., Tomasi, J., Barone, V., Mennuccii, B., Cossi, M., Scalmani, G., Rega, N., Petersson, G. A., Nakatsuji, H., Hada, M., Ehara, M., Toyota, K., Fukuda, R., Hasegawa, J., Ishida, M., Nakajima, T., Honda, Y., Kitao, O., Nakai, H., Klene, M., Li, X. Y., Knox, J. E., Hratchian, H. P., Cross, J. B., Adamo, C., Jaramillo, J., Gomperts, R., Stratmann, R. E., Yazyev, O., Austin, A. J., Cammi, R., Pomelli, C., Ochterski, J. W., Ayala, P. Y., Morokuma, K., Voth, G. A., Salvador, P., Dannenberg, J. J., Zakrzewski, V. G., Dapprich, S., Daniels, A. T., Strain, M. C., Farkas, O., Malick, D. K., Rabuck, A. D., Raghavachari, K., Foresman, J. B., Ortiz, J. V., Cui, Q., Baboul, A. G., Clifford, S., Cioslowski, J., Stefanov, B. B., Liu, G., Liashenko, A., Piskorz, P., Komaromi, I., Martin, R. L., Fox, D. J., Keith, T., Al-Laham, M. A., Peng, C. Y., Nanayakkara, A., Challacombe, M., Gill, P. M. W., Johnson, B. G., Chen, W., Wong, M. W., Gonzalez, C. and Pople, J. A. (2003) Gussian 03, Revision A.1, Gaussian, Inc., Pittsburgh, PA
30 Xin, Y., Gadda, G. and Hamelberg, D. (2009) The cluster of hydrophobic residues controls the entrance to the active site of choline oxidase. Biochemistry, **48,** 9599-9605
31 Fishelovitch, D., Shaik, S., Wolfson, H. J. and Nussinov, R. (2009) Theoretical characterization of substrate access/exit channels in the human cytochrome P450 3A4 enzyme: Involvement of phenylalanine residues in the gating mechanism. J.Phys.Chem.B, **113,** 13018-13025
32 Meyer, E. A., Castellano, R. K. and Diederich, F. (2003) Interactions with aromatic rings in chemical and

biological recognition. Angew.Chem.Int.Ed., **42,** 1210-1250
33 Dinadayalane, T. C. and Leszczynski, J. (2009) Geometries and stabilities of various configurations of benzene dimer: details of novel V-shaped structure revealed. Struct.Chem., **20,** 11-20
34 Roth, J. P. and Klinman, J. P. (2003) Catalysis of electron transfer during activation of O_2 by the flavoprotein glucose oxidase. Proc.Natl.Acad.Sci.USA, **100,** 62-67
35 Su, Q. and Klinman, J. P. (1999) Nature of oxygen activation in glucose oxidase from *Aspergillus niger*: the importance of electrostatic stabilization in superoxide formation. Biochemistry, **38,** 8572-8581
36 Wohlfahrt, G., Witt, S., Hendle, J., Schomburg, D., Kalisz, H. M. and Hecht, H.-J. (1999) 1.8 and 1.9 Å resolution structures of the *Penicillium amagasakiense* and *Aspergillus niger* glucose oxidase as a basis for modelling substrate complexes. Acta Crystallogr.D, **55,** 969-977
37 Agarwal, P. K., Billeter, S. R. and Hammes-Schiffer, S. (2002) Nuclear quantum effects and enzyme dynamics in dihydrofolate reductase catalysis. J.Phys.Chem.B, **106,** 3283-3293
38 Guallar, V., Harris, D. L., Batista, V. S. and Miller, W. H. (2002) Proton-transfer dynamics in the activation of cytochrome P450eryF. J.Am.Chem.Soc., **124,** 1430-1437
39 Truong, T. N. and McCammon, J. A. (1991) Direct dynamics study of intramolecular proton-transfer in hydrogenoxalate anion. J.Am.Chem.Soc., **113,** 7504-7508
40 Ferreira, P., Hernández-Ortega, A., Herguedas, B., Martínez, A. T. and Medina, M. (2009) Aryl-alcohol oxidase involved in lignin degradation: A mechanistic study based on steady and pre-steady state kinetics and primary and solvent isotope effects with two different alcohol substrates. J.Biol.Chem., **284,** 2480-2487
41 Ferreira, P., Hernández-Ortega, A., Herguedas, B., Rencoret, J., Gutiérrez, A., Martínez, M. J., Jiménez-Barbero, J., Medina, M. and Martínez, A. T. (2010) Kinetic and chemical characterization of aldehyde oxidation by fungal aryl-alcohol oxidase. Biochem.J., **425,** 585-593
42 Newcomb, M., Letadicbiadatti, F. H., Chestney, D. L., Roberts, E. S. and Hollenberg, P. F. (1995) A nonsynchronous concerted mechanism for cytochrome-P-450 catalyzed hydroxylation. J.Am.Chem.Soc., **117,** 12085-12091
43 Fan, F. and Gadda, G. (2005) On the catalytic mechanism of choline oxidase. J.Am.Chem.Soc., **127,** 2067-2074
44 Gadda, G. (2003) pH and deuterium kinetic isotope effects studies on the oxidation of choline to betaine-aldehyde catalyzed by choline oxidase. Biochim.Biophys.Acta, **1650,** 4-9

Biochemical Journal Immediate Publication. Published on 04 Mar 2011 as manuscript BJ20102090

Table 1 Steady and transient-state kinetic parameters of wild-type recombinant AAO and its His^{502} and His^{546} variants in the reaction with *p*-anisyl alcohol as substrate

Steady-state constants for native AAO and its H546S and H546A variants were determined by simultaneously varying the concentrations of *p*-anisyl alcohol and O_2 in 0.1 M phosphate, pH 6, at 25 ºC, while those of the other variants were determined in air-saturated buffer (no O_2-concentration dependence). Steady-state kinetic constants included turnover rates (k_{cat}) and Michaelis constants for the alcohol ($K_{m(Al)}$) and O_2 ($K_{m(O2)}$) measured at 25ºC. Transient-state kinetic constants included reduction (k_{red}) and dissociation (K_d) constants calculated at 12ºC and 25ºC for wild-type AAO and its variants, respectively, using the above buffer.

	AAO	H502S	H502A	H546S	H546A
Steady-state:					
k_{cat} (s^{-1})	208 ± 5	0.069 ± 0.005	0.072 ± 0.002	17 ± 1	3.5 ± 0.1
$K_{m(Al)}$ (μM)	48 ± 3	1289 ± 246	3820 ± 234	310 ± 56	1160 ± 33
$k_{cat}/K_{m(Al)}$ ($mM^{-1}\cdot s^{-1}$)	4330 ± 290	0.054 ± 0.01	0.019 ± 0.001	53 ± 11	3.0 ± 0.1
$K_{m(O2)}$ (μM)	276 ± 19	nd[a]	nd	18 ± 3	6 ± 1
$k_{cat}/K_{m(O2)}$ ($mM^{-1}\cdot s^{-1}$)	754 ± 55	nd	nd	923 ± 149	590 ± 100
Transient-state:					
k_{red} (s^{-1})	139 ± 16	0.111 ± 0.002	0.076 ± 0.001	ins[b]	3.96 ± 0.05
K_d (μM)	26 ± 5	4740 ± 184	3180 ± 74	ins	1310 ± 30

[a] nd, not determined because of no turnover-rate dependence on O_2 concentration; [b] ins, not determined because of H546S instability during stopped-flow determinations

Table 2 Comparison of substrate, solvent, and multiple KIE

The KIE on the apparent k_{cat} and the k_{red} constants for AAO oxidation of α-dideuterated *p*-anisyl alcohol and 2,4-hexadien-1-ol, and CHO oxidation of 1,2-tetradeuterated choline are shown. The substrate KIE ($^{2}H k$) is the ratio between the activity on the non-deuterated and the deuterated substrate; the solvent KIE ($^{2}H_2O k$) is the ratio between the activity in H_2O and $^{2}H_2O$, and the multiple KIE ($^{2}H,^{2}H_2O k$) is the ratio between the activity on the non-deuterated substrate in water and the deuterated substrate in $^{2}H_2O$.

	AAO [a]		CHO [b]
	p-anisyl alcohol	2,4-hexadien-1-ol	choline
$^{2}H k_{cat}$	5.4 ± 0.1	5.6 ± 0.1	7.3 ± 1.0
$^{2}H k_{red}$	9.0 ± 0.8	8.9 ± 0.2	8.9 ± 0.2
$^{2}H_2O k_{cat}$	1.35 ± 0.06	1.25 ± 0.03	1.1 ± 0.1
$^{2}H,^{2}H_2O k_{cat}$	7.0 ± 0.4	7.0 ± 0.2	7.3 ± 0.2
$^{2}H_2O k_{red}$	1.42 ± 0.10	1.33 ± 0.02	0.99 ± 0.02
$^{2}H,^{2}H_2O k_{red}$	13.5 ± 0.9	12.5 ± 0.3	8.4 ± 0.2

[a] From Ferreira *et al.* [40]. [b] From Fan and Gadda [43].

Biochemical Journal Immediate Publication. Published on 04 Mar 2011 as manuscript BJ20102090

FIGURE LEGENDS

Figure 1 Active site in AAO and CHO crystal structures

The FAD isoalloxazine ring and five active-site residues are shown (as CPK sticks). A dimethylsulphoxide (DMS) molecule occupies the CHO substrate binding site, while a water molecule (red sphere) is found at the putative active site of AAO. From PDB entries 3FIM and 2JBV, respectively [7;11].

Figure 2 Energy profile for substrate diffusion into AAO active site obtained with PELE

The axis-x shows the distance of the N5 position of the isoalloxazine ring of FAD to the 2,4-hexadien-1-ol center of mass, and axis-y the internal energies of hundreds of conformations obtained by PELE (points correspond to the different conformations mapped by 12 processors working for 10 h).

Figure 3 Three representative snapshots along substrate diffusion into AAO active site

Three different situations during PELE predicted migration of *p*-anisyl alcohol into the AAO active site are shown. The right panel (**C**) corresponds to a catalytically-active conformation, where we show the proton and hydride transfer coordinates (to His^{502} Nε and isoalloxazine N5, respectively) with pink arrows, while alcohol entrance (**A**) and an intermediate position of the migration trajectory (**B**) are shown in the other panels.

Figure 4 pH dependence of kinetic constants for two mutated AAO variants

Apparent catalytic efficiency ($^{app}(k_{cat}/K_m)$ in $mM^{-1}\cdot min^{-1}$) (**A**) and turnover ($^{app}k_{cat}$ in min^{-1}) (**B**) for *p*-anisyl alcohol oxidation by the H546S and H502S AAO variants were determined at different pH values, under air saturation conditions at 25 ºC, and presented using logarithmic transformation (and two different y axes in **B**).

Figure 5 Putative protonation states of conserved histidines at AAO active site

The three panels show the initial His^{546} protonation state (Hid^{502}/Hip^{546}, with His^{502} only protonated at Nδ and His^{546} doubly protonated) (**A**), the final His^{546} protonation state ($Glh^{389}/Hid^{502}/Hid^{546}$ or simply Glh^{389}/Hid^{502}, with both histidines being only protonated at Nδ and Glu^{389} being protonated) (**B**), and the His^{502} protonation state (Hie^{502}/Hie^{546}, with both histidines being only protonated at Nε) (**C**). The side-chain of His^{546} has been flipped with respect to the deposited crystal structure.

Figure 6 Reaction profiles of *p*-anisyl alcohol and 2,4-hexadien-1-ol dehydrogenation by AAO

QM/MM energy profiles obtained for the reactions of AAO with *p*-anisyl alcohol (**A**) and 2,4-hexadien-1-ol (**B**). In these computations, two protonation states of Glu^{389}, His^{502} and His^{546} (**B** and **C** in **Figure 5**) and two orders or the hydride+proton transfer reaction were considered in the following combinations: **i)** $Glh^{389}/Hid^{502}/Hid^{546}$ state and reaction initiated by proton transfer (■); **ii)** $Glh^{389}/Hid^{502}/Hid^{546}$ and reaction initiated by hydride transfer (♦); **iii)** Hie^{502}/Hie^{546} state and reaction initiated by proton transfer (**x**); and **iv)** Hie^{502}/Hie^{546} state and reaction initiated by hydride transfer (▲). The course of the reaction, from left to right on axis-x, was estimated as the total distance between the alcohol hydroxyl hydrogen and the catalytic histidine (H^+ transfer) plus the distance between its benzylic hydrogen and the flavin N5 (H^- transfer).

Figure 7 Energy profiles for *p*-anisyl alcohol oxidation by AAO and choline oxidation by CHO

The energy profiles for *p*-anisyl alcohol oxidation by AAO (■) and choline oxidation by CHO (**x**), in reactions initiated by proton transfer to the catalytic base (His^{502} and His^{466}, respectively) followed by hydride transfer to flavin N5, were obtained by QM/MM calculations. The course of the reaction, from left to right on axis-x, was estimated as the total distance between the alcohol hydroxyl hydrogen and the catalytic histidine (H^+ transfer) plus the distance between its benzylic hydrogen and the flavin N5 (H^- transfer).

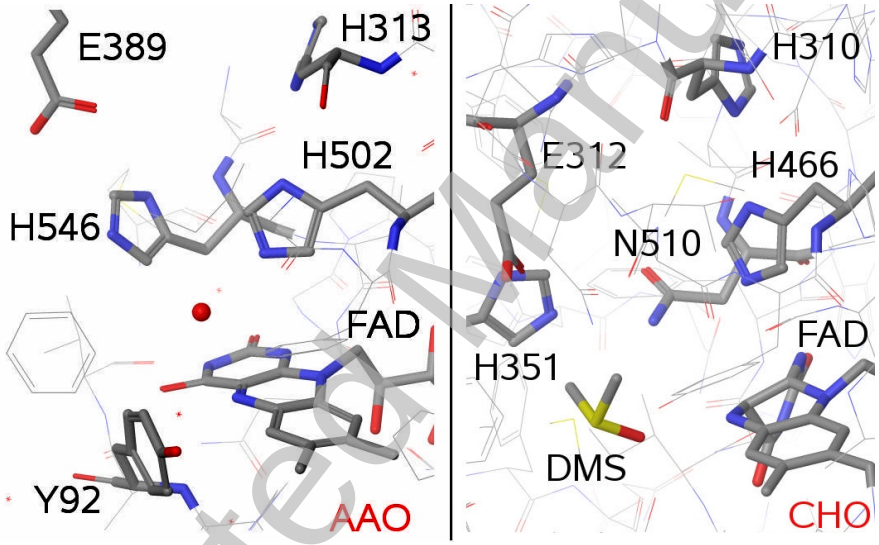

Fig 1

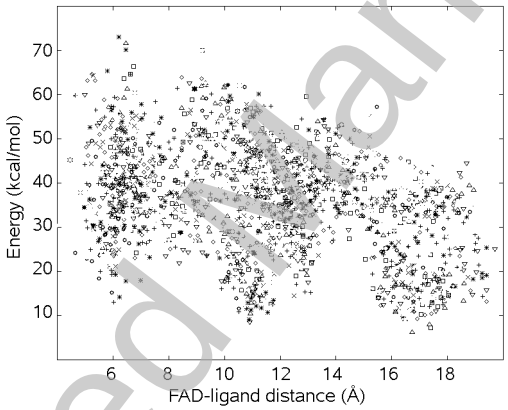

Fig 2

Biochemical Journal Immediate Publication. Published on 04 Mar 2011 as manuscript BJ20102090

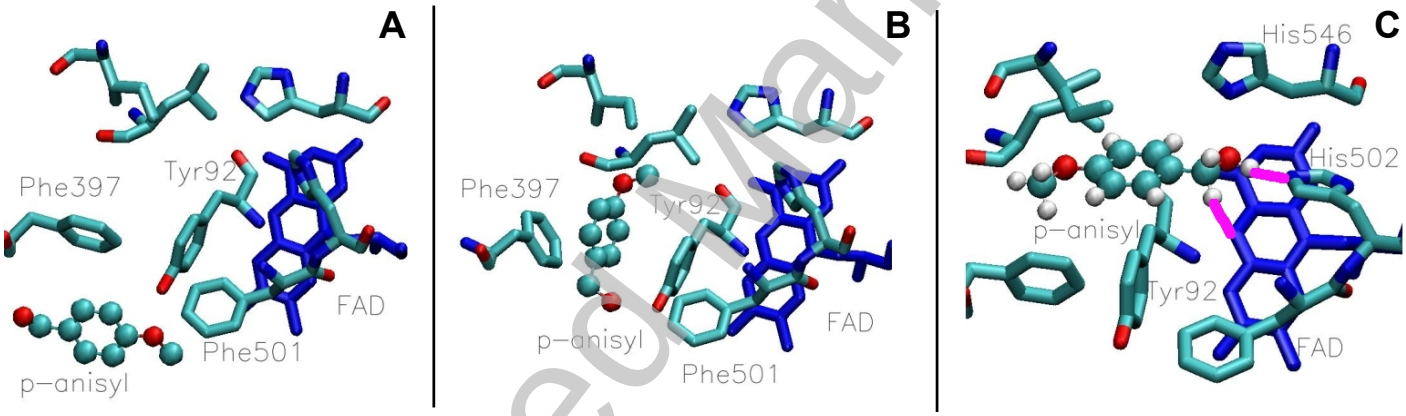

Fig 3

Biochemical Journal Immediate Publication. Published on 04 Mar 2011 as manuscript BJ20102090

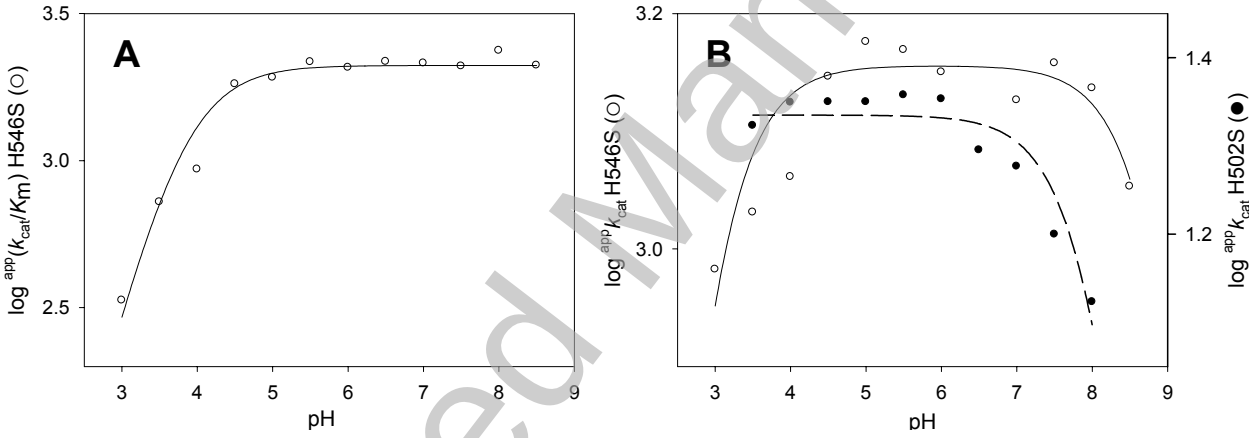

Fig 4

Biochemical Journal Immediate Publication. Published on 04 Mar 2011 as manuscript BJ20102090

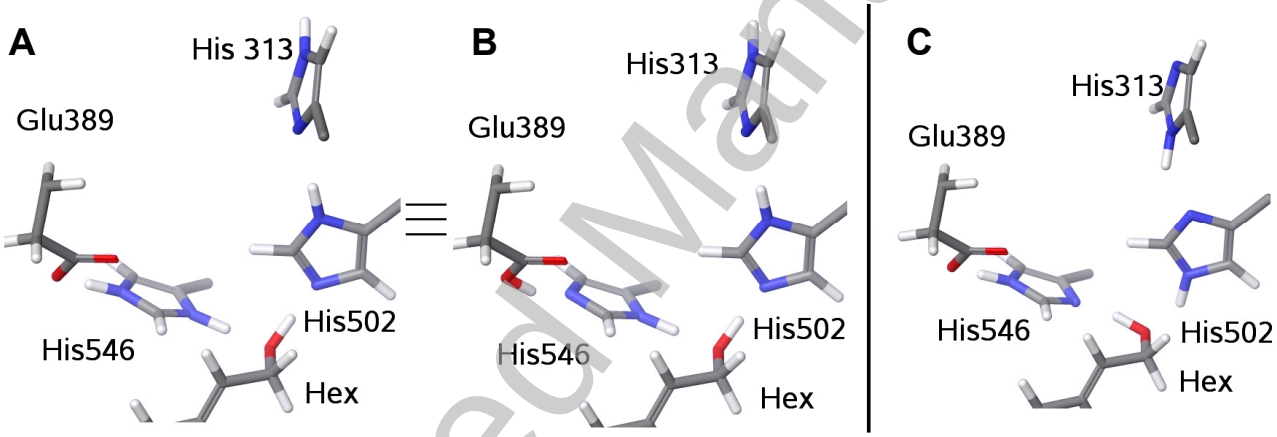

Fig 5

Biochemical Journal Immediate Publication. Published on 04 Mar 2011 as manuscript BJ20102090

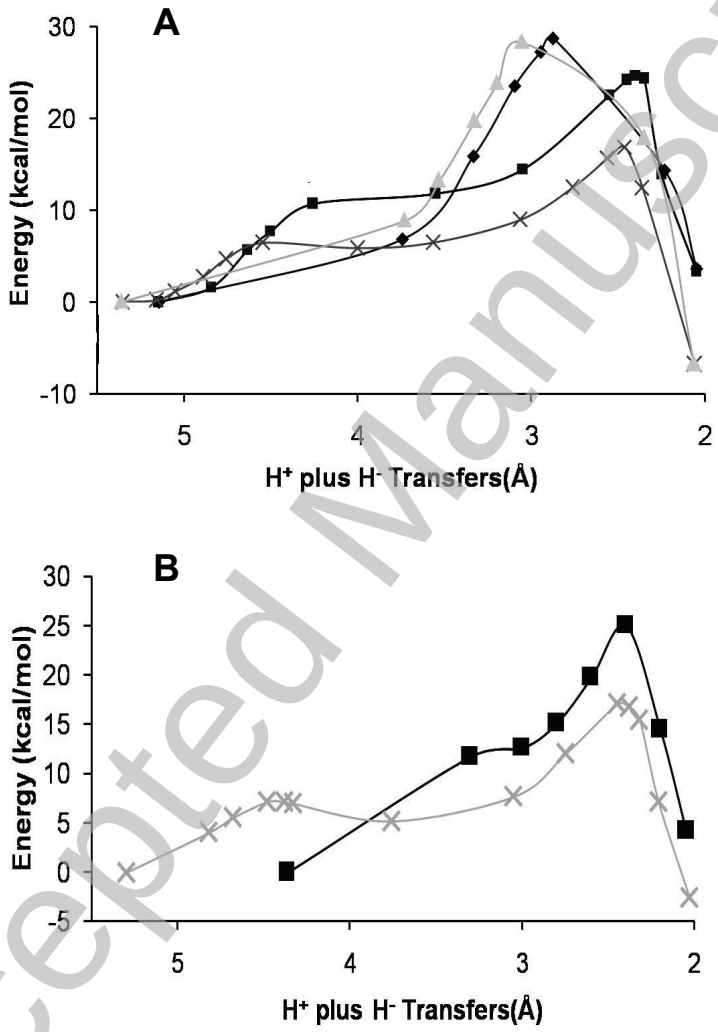

Fig 6

Biochemical Journal Immediate Publication. Published on 04 Mar 2011 as manuscript BJ20102090

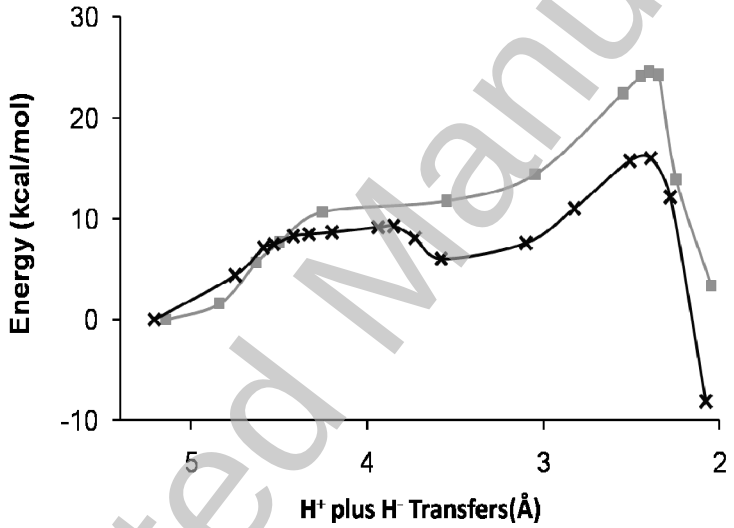

Fig 7